Acta Mech 227, 1251–1264 (2016)
DOI 10.1007/s00707-015-1555-4

ORIGINAL PAPER

Hua-nan Xu · Zai-lin Yang · Sha-sha Wang

Dynamics response of complex defects near bimaterials interface by incident out-plane waves

Received: 21 September 2015 / Revised: 4 December 2015 / Published online: 12 January 2016

Abstract Dynamics response of an elliptical cavity and a crack (on different sides) near bimaterials interface under incident out-plane waves is studied by applying the methods of complex variables and Green's function. Firstly, based on "conjunction," the analytical model is divided along the horizontal interface into an elastic half-plane possessing an elliptical cavity and a full elastic half-plane containing a crack. Using complex variables, the scattering displacement field of the half-plane containing an elliptical cavity under incident out-plane waves is then derived. According to the method of Green's function, the corresponding Green's functions of two half-planes impacted by an out-plane source load are further deduced. Combined with "crack division," a crack at the full elastic the half-plane is created, and thus, expressions of displacement and stress are derived while the cavity coexists with the crack. Undetermined antiplane forces are loaded on the horizontal surfaces for conjunction of two sections and then solved by a series of Fredholm integral equations on account of continuity conditions of the interface. Finally, this paper focuses on the discussion of the influence law of different parameters on the dynamics response of complex defects near bimaterials interface by comprehensive numerical results.

1 Introduction

Interface is common in engineering practice and underground exploration engineering, such as underground strata, laminates, composites, polycrystal composites, various bonding structures and so on. In nature, defects (cavity, inclusion and crack) are always clustered around underground strata, and flaws usually occur at the region where a material property varies acutely in a medium or structure namely the surface or the vicinity of an interface. The scattering wave caused by defects near interface involves various characteristic parameters of defects, such as shape, size and location, namely the elastic wave inversion, which can provide a theoretical basis for applications such as geophysical prospecting, earthquake engineering, nondestructive testing, and flaw detection of material (NDT).

On interface problem, a certain amount of studies has been carried out [1–19]. The pioneer one can be traced to C.G. Knott's report, in 1899, on reflection and diffraction phenomenon of an elastic wave in interface.

H. Xu · Z. Yang (✉) · S. Wang
College of Aerospace and Civil Engineering, Harbin Engineering University, Harbin, China
E-mail: yangzailin00@163.com

H. Xu · S. Wang
School of Resource Engineering, Longyan University, Longyan, China
E-mail: hntiger_86@126.com

S. Wang
E-mail: w275287712@126.com

Approximately three decades later, Stoneley drew a conclusion that a surface wave (Stoneley wave) existed along the interface constituted by two half-planes.

In recent decades, ascribed to the delamination character of the earth medium, the wave propagation issue in a solid interface increasingly fascinates researchers. The complex variables theory is one of most commonly used methods and has become popular in elastic wave scattering analyses since first used by Liu et al. [2] for the solution of static stress concentration around an irregularly shaped cavity in an infinite elastic plane. Subsequently, Chen et al. [3] solved upright incident SH-waves at a semicylindrical interface with a circular lining structure. Wang et al. [4] addressed steady SH-wave scattering and performed a dynamic analysis of multiple circular cavities in half-space. Xu et al. [5] derived an analytical solution for the scattering of plane SH-waves by two separated circular tunnel linings. Liu et al. [6] presented a theoretical study of SH-wave scattering by cavities in the neighborhood of a bimaterials interface. Combined with crack division and weakly singular integral equation method, Liu et al. [7] obtained the solution of the scattering of SH-waves by an interface linear crack and a circular cavity near a bimaterials interface. Yang et al. [8,9] successively solved the problem of the scattering of an SH-wave by an interacting mode III crack and an inclusion, an elastic cylindrical inclusion and a crack in a half-space. In combination with the integral transform method, Lu et al. [10] developed a hypersingular integral equation and Green's function to discuss SH-wave scattering by cracks in bimaterials interface.

In addition, some other important approaches have also been carried out by many contributions. Rodriguez-Castellanos et al. [11] employed a numerical approach using a boundary integral formulation to study diffraction of seismic waves in an elastic cracked half-plane. Tsaur et al. [12] implemented the region-matching technique to derive a series solution to the SH-wave scattering problem of an embedded truncated circular cavity, which could provide references for the earthquake-resistant design methods of underground structures. Scattering of SH-waves by an embedded rigid elliptic cylinder of finite length, which is partially debonded from elastic soil, is studied by Wang et al. [13] in application of the wave function expansion method. Coussy [14] used a method of perturbation to derive an integral representation of the displacement field for the scattering of a plane wave from an inclusion with an interface crack. Bair and David [15] employed a probabilistic method to analyze two-dimensional wave scattering by surface-breaking cracks and cavities. With direct boundary integral equation method, Tanimura [16] analyzed stress wave propagation in elastic/viscoplastic cylindrical bodies containing a spherical cavity, Yu et al. [17] solved scattering of plane harmonic P, SV and Rayleigh waves by a completely embedded corrugated elastic inclusion, and Dravinski et al. [18] investigated SH-waves scattering by any number of inclusions with general shape and position in elastic half-space. The direct boundary element method (BEM) was developed for studying the elastic wave fields in an isotropic half-plane with free-surface relief, unlined and lined tunnels, and multiple buried inclusions[19].

A study on the elastic wave scattering problem by elliptical cavities and cracks near bimaterials interface is one of the foundation subjects in elastodynamics. It can be widely used for modern acoustics, geophysics, explosion mechanics and research on material mechanical properties, such as the fields of oil exploration, underground tunnel engineering, mineral resources exploration, QNDE, radar, sonar and explosion. In most published works, the model of cavities was assumed to be a circular one for convenient investigation, whereas the irregularly shaped cavities are much more common in practical engineering. Thus, more research is still required to provide worthy records to be referenced in engineering mentoring. To date, little investigation has been reported on this topic. The aim of this paper is to develop the methods of Green's function and complex variables to investigate the SH-wave scattering by an elliptical cavity and a crack near bimaterials interface. The key analytical tool is applying the method of "conformal mapping" in complex variables to map the outland of the elliptical boundary of the cavity in Z-plane to one of the unit circle boundary in η-plane.

2 Problem statement

Figure 1 shows the analytical model of an elliptical cavity and a crack in different media near bimaterials interface. The medium I represents an elastic half-plane containing an elliptical cavity with an incident wave $W_{\mathrm{I}}^{(i)}$ from downside, while the medium II another half-plane possessing a beeline crack. Another incident wave $W_{\mathrm{II}}^{(i)}$ from upward side is symmetrical with $W_{\mathrm{I}}^{(i)}$ about x' axis. Suppose that the material parameters of the media are defined as $(\rho_{1,}\mu_{1;}\rho_{2,}\mu_{2})$, and the length of crack $l = 2A$. Three given coordinates: xoy, x_1oy_1

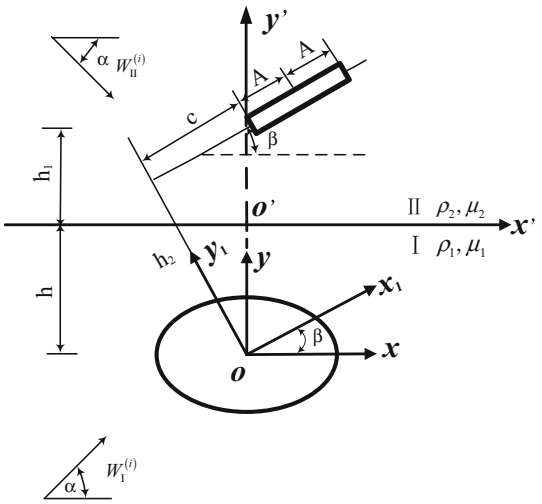

Fig. 1 Model of an elliptical cavity and a crack in different media near bimaterials interface

and $x'o'y'$, are related by

$$\begin{aligned} &x' = x, \quad y' = y - h, \\ &x_1 = x\cos\beta + y\sin\beta, \quad y_1 = y\cos\beta - x\sin\beta, \\ &h_2 = (h + h_1 - c\sin\beta)/\cos\beta. \end{aligned} \tag{1}$$

3 Governing equations

In an isotropic medium, the scattering of an SH-wave is the simplest one of the study on elastic wave scattering problems. In the complex plane $(z, \bar{z})$, the displacement field W excited by SH-waves obeys

$$\frac{\partial^2 W}{\partial z \partial \bar{z}} + \frac{1}{4}k^2 W = 0 \tag{2}$$

where $k = \omega/c_s$, in which ω is the circular frequency of the wave function, $c_s = \sqrt{\mu/\rho}$ the propagation velocity of the shear wave, and ρ and μ the mass density and shear modulus of the medium, respectively.

The corresponding stresses are given by

$$\begin{aligned} \tau_{rz} &= \mu\left(\frac{\partial W}{\partial z}e^{i\theta} + \frac{\partial W}{\partial \bar{z}}e^{-i\theta}\right), \\ \tau_{\theta z} &= i\mu\left(\frac{\partial W}{\partial z}e^{i\theta} - \frac{\partial W}{\partial \bar{z}}e^{-i\theta}\right). \end{aligned} \tag{3}$$

Introducing the conformal mapping function: $z = w(\eta) = R(\eta + m/\eta)$ ($\eta = Re^{i\theta}$, $R = (a+b)/2$, $m = (a-b)/(a+b)$, a and b, respectively, represent the length of the semi-major axis and semi-minor axis), the outland of the elliptical boundary in the Z-plane is mapped to one of unit circle boundary in the η-plane, as shown in Fig. 2.

Consequently, Eq. (2) is transformed into an expression with respect to the variable η and the conjugate $\bar{\eta}$,

$$\frac{1}{w'(\eta)\overline{w'(\eta)}}\frac{\partial^2 W}{\partial \eta \partial \bar{\eta}} + \frac{k^2}{4}W = 0. \tag{4}$$

The corresponding stresses turn into

$$\begin{aligned} \tau_{rz} &= \frac{\mu}{R\,|w'(\eta)|}\left(\eta\frac{\partial W}{\partial \eta} + \bar{\eta}\frac{\partial W}{\partial \bar{\eta}}\right), \\ \tau_{\theta z} &= \frac{i\mu}{R\,|w'(\eta)|}\left(\eta\frac{\partial W}{\partial \eta} - \bar{\eta}\frac{\partial W}{\partial \bar{\eta}}\right). \end{aligned} \tag{5}$$

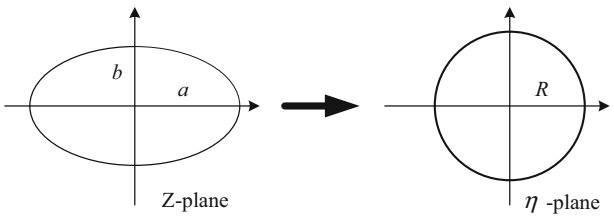

Fig. 2 "Conformal mapping" of ellipse

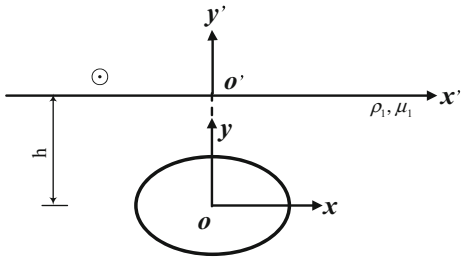

Fig. 3 Half-plane model of elliptical cavity impacted by an out-plane source load at the surface

4 The scattering wave around the elliptical cavity

Based on the symmetry of the scattering wave and multipolar coordinates, the scattering wave $W_{\mathrm{I}}^{(s)}$ around the elliptical cavity can be constructed, which should obey the governing Eq. (2) and the radiation condition for infinite distance except the stress-free condition on the horizontal interface.

Under conformal mapping, $W_{\mathrm{I}}^{(s)}$ takes the form of

$$W_{\mathrm{I}}^{(s)} = \sum_{n=-\infty}^{\infty} A_n \left\{ H_n^{(1)}\left(k_1 \left|w(\eta)\right|\right) \left[\frac{w(\eta)}{|w(\eta)|}\right]^n + H_n^{(1)}\left(k_1 \left|w(\eta) - 2hi\right|\right) \left[\frac{w(\eta) - 2hi}{|w(\eta) - 2hi|}\right]^{-n} \right\} \tag{6}$$

where A_n are the unknown coefficients to be determined by the boundary condition of the elliptical cavity.

Inserting the expression above into Eq. (5), the relevant stresses can be derived.

5 Green's function

5.1 Green's function G_1

The first Green's function in the current paper is the displacement field of the half-plane of elliptical cavity impacted by an out-plane source load at the surface, marked as G_1. The analysis model is given in Fig. 3, which has boundary conditions as follows:

$$\begin{cases} \tau_{rz} = 0, & \eta = \mathrm{e}^{i\theta}(R = 1) \\ \tau_{\theta z} = \delta(z - z_0), & \theta = 0, \pi \end{cases}. \tag{7}$$

In an elastic half-plane, the wave $G_1^{(i)}$ excited by the out-plane line load $\delta(z - z_0)$ can be regarded as an incident wave, and in the mapping plane, it is defined as

$$G_1^{(i)} = \frac{i}{2\mu} H_0^{(1)}\left(k \left|w(\eta) - w(\eta_0)\right|\right) \tag{8}$$

where $H_0^{(1)}(\cdot)$ is the 0th-order Hankel function of the first kind, and η_0 the image point of z_0 in the mapping plane.

The scattering waves $G_{\mathrm{I}}^{(s)}$ caused by the elliptical cavity can be given as Eq. (6).

Now, the total wave field has been derived,

$$G_1 = G_1^{(i)} + G_1^{(s)}. \tag{9}$$

Substitution of the expression (9) into Eq.(5), the corresponding stresses can be obtained.

Inserting the expressions of displacements and stresses into the boundary conditions (7), we have

$$\sum_{n=-\infty}^{+\infty} A_n \varepsilon_n = \varepsilon \tag{10}$$

where

$$\varepsilon = i H_1^{(1)}(k\,|w(\eta) - w(\eta_0)|)\left[\frac{\bar{w}(\eta) - \bar{w}(\eta_0)}{|w(\eta) - w(\eta_0)|}\frac{\eta w'(\eta)}{R\,|w'(\eta)|} + \frac{w(\eta) - w(\eta_0)}{|w(\eta) - w(\eta_0)|}\frac{\bar{\eta}\bar{w}'(\eta)}{R\,|w'(\eta)|}\right],$$

$$\varepsilon_n = 2\mu\left\{\left[H_{n-1}^{(1)}(k\,|w(\eta)|)\left[\frac{w(\eta)}{|w(\eta)|}\right]^{n-1} - H_{n+1}^{(1)}(k\,|w(\eta) - 2ih|)\left[\frac{w(\eta) - 2ih}{|w(\eta) - 2ih|}\right]^{-(n+1)}\right]\frac{\eta w'(\eta)}{R\,|w'(\eta)|}\right.$$
$$\left. - \left[H_{n+1}^{(1)}(k\,|w(\eta)|)\left[\frac{w(\eta)}{|w(\eta)|}\right]^{n+1} - H_{n-1}^{(1)}(k\,|w(\eta) - 2ih|)\left[\frac{w(\eta) - 2ih}{|w(\eta) - 2ih|}\right]^{-(n-1)}\right]\frac{\bar{\eta}\bar{w}'(\eta)}{R\,|w'(\eta)|}\right\}.$$

Multiplying both of the sides by $\mathrm{e}^{-im\theta}$ and integrating over the interval $(-\pi, \pi)$, a set of infinite algebraic equations to determine the coefficients A_n can be obtained,

$$\sum_{n=-\infty}^{+\infty} A_n \varepsilon_{mn} = \varepsilon_m, \tag{11}$$

in which $\varepsilon_{mn} = \frac{1}{2\pi}\int_{-\pi}^{\pi} \varepsilon_n \mathrm{e}^{-im\theta}\mathrm{d}\theta$, $\varepsilon_m = \frac{1}{2\pi}\int_{-\pi}^{\pi} \varepsilon \mathrm{e}^{-im\theta}\mathrm{d}\theta$.

5.2 Green's function G_2

In the elastic half-plane II, the wave field $G_2^{(i)}$ excited by the out-plane line load $\delta\left(z' - z_0'\right)$ and the reflected wave $G_2^{(r)}$ caused by the surface can be described in the following forms:

$$G_2^{(i)} = \frac{i}{4\mu_2} H_0^{(1)}\left(k_2\left|z' - z_0'\right|\right), \tag{12}$$

$$G_2^{(r)} = \frac{i}{4\mu_2} H_0^{(1)}\left(k_2\left|z' - \bar{z}_0'\right|\right), \tag{13}$$

in which $H_0^{(1)}(\cdot)$ is the 0th-order Hankel function of the first kind, z_0' indicates the source point and $\bar{z}_0'$ the complex conjugate.

The total wave field in the elastic half-plane II, namely the Green's function G_2 in this Section, can be written as

$$G_2 = G_2^{(i)} + G_2^{(r)}. \tag{14}$$

5.3 Green's function G_3

The wave field caused by the out-plane line load $\delta\left(z' - z_0'\right)$ in a full elastic half-plane II is defined as G_3, which can be deemed to be an incident wave,

$$G_3 = \frac{i}{2\mu_2} H_0^{(1)}\left(k_2\left|z' - z_0'\right|\right). \tag{15}$$

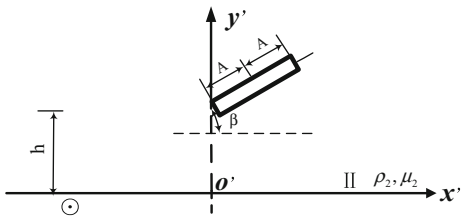

Fig. 4 Half-plane model of a crack impacted by an out-plane source load at surface

5.4 Green's function G_4

As given in Fig. 4, the fourth Green's function indicates the displacement field for the half-plane II containing a beeline crack impacted by an out-plane source load at surface, marked as G_4.

The wave field G_3 caused by an out-plane source load at surface half-plane II has been derived in Sect. 5.3.

Combined with the Green's function G_2 obtained in Sect. 5.2, the displacement field $G_{\mathrm{II}}^{(c)}$ caused by infliction of antiplane forces to create a crack can be deduced,

$$G_{\mathrm{II}}^{(c)} = \int_l \tau_{\theta' z'} G_2 \mathrm{d}l. \tag{16}$$

Then, the total wave field in this Section is obtained,

$$G_4 = G_3 - G_{\mathrm{II}}^{(c)}. \tag{17}$$

6 Scattering by an elliptical cavity and a crack near bimaterials interface

6.1 Incident SH-waves

Interaction of an elliptical cavity and a crack near bimaterials interface under incident SH-waves can be regarded as "conjunction" problem to investigate. Firstly, along the interface $y = h$, we subdivide the bimaterials into elastic half-plane I and II with different material constants $(\rho_1, \mu_1; \rho_2, \mu_2)$, in which I possesses an elliptical cavity and II a full elastic space containing a crack.

In medium I, $W^{(i)}$ and $W^{(r)}$ are described in the following forms:

$$W^{(i)} = W_0 \exp\left\{\frac{ik_1}{2}\left[(z - ih)\,\mathrm{e}^{-i\alpha} + (\bar{z} + ih)\,\mathrm{e}^{i\alpha}\right]\right\}, \tag{18}$$

$$W^{(r)} = W_0 \exp\left\{\frac{ik_1}{2}\left[(z - ih)\,\mathrm{e}^{i\alpha} + (\bar{z} + ih)\,\mathrm{e}^{-i\alpha}\right]\right\}, \tag{19}$$

where W_0 is the maximum amplitude of the incident wave and α denotes the incident angle.

6.2 The wave field in district I and II

The scattering wave $W_{\mathrm{I}}^{(s)}$ excited by the elliptical cavity in half-plane is given by Eq. (6).

Then, the total wave field of half-plane I containing an elliptical cavity is derived,

$$W_{\mathrm{I}}^{(t)} = W^{(i)} + W^{(r)} + W_{\mathrm{I}}^{(s)}. \tag{20}$$

Introducing the mapping function $z = \omega(\eta)$, in mapping plane η, the incident wave $W^{(i)}$ and the reflected wave $W^{(r)}$ are transformed into

$$W^{(i)} = W_0 \exp\left\{\frac{ik_1}{2}\left[(w(\eta) - ih)\,\mathrm{e}^{-i\alpha} + \left(\overline{w(\eta)} + ih\right)\mathrm{e}^{i\alpha}\right]\right\},$$

$$W^{(r)} = W_0 \exp\left\{\frac{ik_1}{2}\left[(w(\eta) - ih)\,\mathrm{e}^{i\alpha} + \left(\overline{w(\eta)} + ih\right)\mathrm{e}^{-i\alpha}\right]\right\}. \tag{21}$$

The corresponding stresses can be obtained by substitution of Eq. (21) into Eq. (5).

With regard to half-plane II, the expression of the incident wave $W_{\mathrm{II}}^{(i)}$ and the reflected wave $W_{\mathrm{II}}^{(r)}$ is uniform in form but different in parameters and opposite in angle with $W_{\mathrm{I}}^{(i)}$ and $W_{\mathrm{I}}^{(r)}$ in the half-plane I

$$\begin{aligned} W_{\mathrm{II}}^{(i)} &= W_0 \exp\left\{\frac{ik_2}{2}\left[(z-ih)\,\mathrm{e}^{i\alpha} + (\bar{z}+ih)\,\mathrm{e}^{-i\alpha}\right]\right\}, \\ W_{\mathrm{II}}^{(r)} &= W_0 \exp\left\{\frac{ik_2}{2}\left[(z-ih)\,\mathrm{e}^{-i\alpha} + (\bar{z}+ih)\,\mathrm{e}^{i\alpha}\right]\right\}. \end{aligned} \tag{22}$$

Then, the total wave field of the elastic half-plane II without crack is

$$W_{\mathrm{II}} = W_{\mathrm{II}}^{(i)} + W_{\mathrm{II}}^{(r)} \tag{23}$$

where $k_2 = \omega/c_2$ stands for the wave number of the medium II, $c_2 = \sqrt{\mu_2/\rho_2}$ the propagation velocity.

Substituting the above expression into Eq. (3), we obtain the relevant stresses $\tau_{\theta z,\mathrm{II}}$.

Subsequently, the total stresses of an arbitrary point in the half-plane can be solved when the surface bears an out-plane harmonic line load. Based on "crack-division" method, if additional stresses with the same magnitude and opposite direction as the total stresses are applied at the same point, the ultimate stresses of this point are zero, and consequently, a crack will be created when a pair of forces with the same magnitude and opposite direction is loaded along the region where the crack will appear. Using the Green's function G_2 derived in Sect. 5.2, the wave field produced in creating a crack by means of antiplane loads' infliction, which is indicated as $W^{(c)}$, is expressed as

$$W^{(c)} = \int_{(c,h_2)}^{(2A+c,h_2)} \tau_{\theta z,\mathrm{II}} G_2 \mathrm{d}z_1. \tag{24}$$

Subtracting Eq. (24) from Eq. (23), we can obtain the total wave field of the half-plane II,

$$W_{\mathrm{II}}^{(t)} = W_{\mathrm{II}}^{(i)} + W_{\mathrm{II}}^{(r)} - W^{(c)}. \tag{25}$$

6.3 Definite integral equations

In a previous paper, the total wave fields of two half-planes have been derived, and the wave field for an elliptical cavity and a crack near bimaterials interface can be deduced based on "conjunction" combining with Green's function, and hence, a series of definite integral equations for the problem is obtained.

On "subdivision" surface $y = h$ of half-plane I, we define the total displacement as $W_{\mathrm{I}}^{(t)}$. Note that the stresses of the incident wave, the reflection wave, the scattering waves of the lining, and the wave field caused by construction of the crack are free in the interface, hence we have

$$\tau_{\theta z,\mathrm{I}}^{(t)} = 0, \theta = 0, \pi. \tag{26}$$

Likewise, on "subdivision" surface of half-plane II, total stress and displacement of "subdivision" surface in half-plane II are:

$$\tau_{\theta z,\mathrm{II}}^{(t)} = 0, \ \theta = 0, \pi. \tag{27}$$

The key to solving this problem is the conjunction of two divided half-planes. To guarantee continuous conditions of displacement and stress at the "subdivision" interface, the horizontal surfaces of the medium I

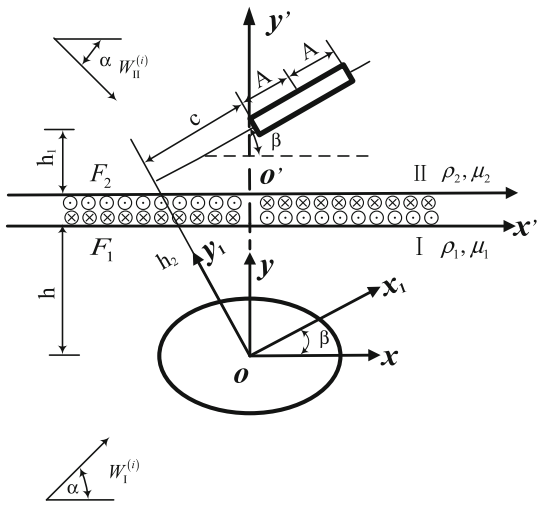

Fig. 5 The conjunction model of "subdivision" surface

and medium II are loaded with a series of undetermined antiplane forces $F_1(r_0, \theta_0)$ and $F_2(r_0, \theta_0)$ (as shown in Fig. 5). Consequently, the total displacements and total stresses of the horizontal surfaces transform into

$$W_{\mathrm{I}} = W_{\mathrm{I}}^{(i)} + W_{\mathrm{I}}^{(r)} + W_{\mathrm{I}}^{(s)} + \int_0^\infty F_1(r_0, \pi)\, G_1(r_1, \theta_1; r_0, \pi)\mathrm{d}r_0 + \int_0^\infty F_1(r_0, 0)\, G_1(r_1, \theta_1; r_0, 0)\mathrm{d}r_0, \tag{28}$$

$$W_{\mathrm{II}} = W_{\mathrm{II}}^{(i)} + W_{\mathrm{II}}^{(r)} - W^{(c)} + \int_0^\infty F_2(r_0, \pi)\, G_4(r_1, \theta_1; r_0, \pi)\mathrm{d}r_0 + \int_0^\infty F_2(r_0, 0)\, G_4(r_1, \theta_1; r_0, 0)\mathrm{d}r_0, \tag{29}$$

$$\tau_{\theta z}^{(\mathrm{I})} = F_1(r_0, \theta_0), \tag{30}$$

$$\tau_{\theta z}^{(\mathrm{II})} = F_2(r_0, \theta_0) \tag{31}$$

where G_1 and G_4 are defined by Eqs. (9) and (17), respectively, $r_1 \mathrm{e}^{i\theta_1} = z' = x' + y'i$, and $r_0 = x'$.

According to the stress balance condition at interface $\tau_{\theta z}^{(\mathrm{I})} = \tau_{\theta z}^{(\mathrm{II})}$, we have

$$F_1(r_0, \theta_0) = F_2(r_0, \theta_0). \tag{32}$$

Combined with expressions (28) and (29), the continuity conditions of displacements at the interface turn to be

$$\begin{aligned} &\int_0^\infty F_1(r_0, \pi)\,[G_1(r_1, \pi; r_0, \pi) + G_4(r_1, \pi; r_0, \pi)]\mathrm{d}r_0 \\ &+ \int_0^\infty F_1(r_0, 0)\,[G_1(r_1, \pi; r_0, 0) + G_4(r_1, \pi; r_0, 0)]\mathrm{d}r_0 \\ &= -\left[W_{\mathrm{I}}^{(i)} + W_{\mathrm{I}}^{(r)} + W_{\mathrm{I}}^{(s)} + W_{\mathrm{II}}^{(i)} + W_{\mathrm{II}}^{(r)} - W^{(c)}\right]_{\theta=\pi}, \end{aligned} \tag{33}$$

$$\begin{aligned} &\int_0^\infty F_1(r_0, \pi)\,[G_1(r_1, \pi; r_0, \pi) + G_4(r_1, \pi; r_0, \pi)]\mathrm{d}r_0 \\ &+ \int_0^\infty F_1(r_0, 0)\,[G_1(r_1, \pi; r_0, 0) + G_4(r_1, \pi; r_0, 0)]\mathrm{d}r_0 \\ &= -\left[W_{\mathrm{I}}^{(i)} + W_{\mathrm{I}}^{(r)} + W_{\mathrm{I}}^{(s)} + W_{\mathrm{II}}^{(i)} + W_{\mathrm{II}}^{(r)} - W^{(c)}\right]_{\theta=0}. \end{aligned} \tag{34}$$

The above definite integral equations belong to the first species Fredholm equations with weak singularity in the semi-infinite domain. According to attenuation characteristics of the scattering wave, the direct discrete

method of weak singular integral equations is adopted here to transform the integral equations into linear algebraic equations for solving the additional forces F_1 and F_2 at a series of discrete points.

7 Dynamic stress concentration factor (DSCF) and dynamic stress intensity factor(DSIF)

When stress-free condition is given at the surface around the elliptical cavity, usually the dynamic stress concentration factor (DSCF) $\tau^*_{\theta z}$ can be written as

$$\tau^*_{\theta z} = \left|\tau^{(\cdot)}_{\theta z}/\tau_0\right| \tag{35}$$

where $\tau^{(\cdot)}_{\theta z}$ is the stress around the outer boundary of the elliptical cavity; $\tau_0 = \mu_1 k_1 W_0$ stands for the largest amplitude of the incident stresses.

In simulation, a non-dimensional dynamic stress intensity factor is usually defined as

$$k_3 = \left|\frac{\tau_{rz}|_{\vec{r}=\vec{r}_0}}{\tau_0 Q}\right| \tag{36}$$

where $\tau_{rz}|_{\vec{r}=\vec{r}_0}$ adopts the nominal stress of small distances in the adjacent area of the crack, Q indicates a characteristic parameter of square root dimension with respect to length, $Q = \sqrt{A}$, and τ_0 represents the maximum stress caused by harmonic wave $W^{(i)}$ incident along α direction, namely $\tau_0 = W_0\mu_1 k_1$.

8 Numerical results and discussion

In the current paper, the algebraic equations to determine the unknown coefficients A_n were solved by truncation limited items to control accuracy. It has been verified that the accuracy to satisfy the zero-stress condition at the elliptical cavity boundary can achieve 10^{-7}. In addition, the solved additional forces F_1 and F_2 by the definite integral Eqs. (33) and (34) are also verified to guarantee the displacement precision which can achieve 10^{-15}. Furthermore, when the current analytical model degenerates to the model of a circular cavity near bimaterials interface, the computed results have been verified to be in good agreement with the data obtained in Reference [6].

Based on above theoretical derivation, a large number of numerical examples are given to discuss the dependence of dynamic stress concentration factors around the elliptical cavity and dynamic stress intensity factors at crack tip on different parameters such as the wave number of incident wave $k_1 a$, the incident angle α, the ratio of the distance between the center of the cavity and the horizontal interface to the length of the semi-major axis of the elliptical cavity h/a, the ratio of the distance between the center of the cavity, and the crack tip to the length of the semi-major axis of the elliptical cavity h_1/a, the length of crack $2A$, the vertical distance between the left-hand member of the crack and the center of the cavity c, the location angle of crack β, and two dimensionless parameters k_2/k_1 and μ_1/μ_2. The expressions of DSCF and DSIF are defined by the expressions (35) and (36), respectively. In numerical examples, suppose that $W_0 = 1.0$, $\mu_2 = 1.0$.

1. Figures 6, 7, 8, 9, and 10 show the distribution of the dynamic stress concentration factor $\tau^*_{\theta z}$ around the elliptical cavity with different parameters.

Figure 6 clearly illustrates that the incident wave number $k_1 a$ (ranging from 0.1 to 2.0) impacted significantly on $\tau^*_{\theta z}$ for incident angles of $\alpha = 30°$ and 90°. As shown in Fig. 6b, when SH-waves incident vertically, the distribution of $\tau^*_{\theta z}$ is presented to be of symmetrical characteristic, the values of which achieve a minimum for $k_1 a = 1.0$ when compared to values obtained for $k_1 a = 0.1$, 0.5 and 2.0. Figure 7 describes the variation of $\tau^*_{\theta z}$ vs. k_2/k_1. It can be observed that $\tau^*_{\theta z}$ changes little with different k_2/k_1.

The ratio of the distance between the center of the cavity and the horizontal interface to the length of the semi-major axis of the elliptical cavity h/a also has large influence on $\tau^*_{\theta z}$ around the elliptical cavity. Figure 8 shows the distribution of $\tau^*_{\theta z}$ for h/a =2.0, 5.0, 10.0 and 20.0, when the SH-wave is incident with different angles. Compared with values obtained for $\alpha = 0°$, the increasing values of h/a yield a complicated distribution of $\tau^*_{\theta z}$ when $\alpha = 30°$ and 90°. For vertical incidence, the values of $\tau^*_{\theta z}$ are in direct proportion to h/a, and the maximum occurs at $\theta = 198°$ $\left(\left|\tau^*_{\theta z}\right|_{\max} = 2.16\right)$, as described in Fig. 8b. It can be concluded that the interface interaction effect is clearly manifested.

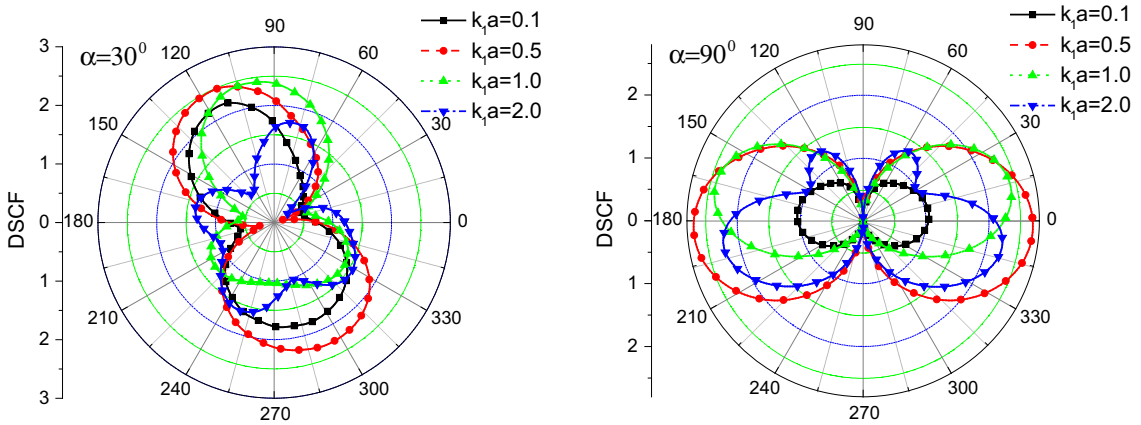

Fig. 6 Variation of DSCF with k_1a ($a = 1.0$, $b = 0.8$, $h/a = 3.0$, $2A = 2.0$, $c = -1.0$, $\beta = 30°$, $k_2/k_1 = 0.5$, $\mu_2/\mu_1 = 0.5$)

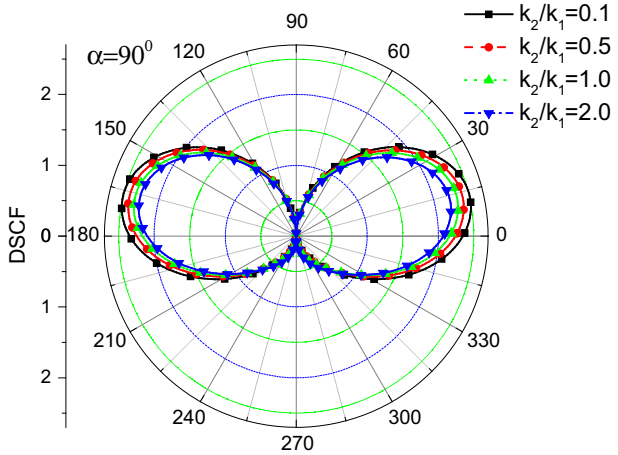

Fig. 7 Variation of DSCF with k_2/k_1 ($a = 1.0$, $b = 0.8$, $h/a = 3.0$, $h_1/a = 3.0$, $c = -1.0$, $2A = 2.0$, $\beta = 30°$, $\mu_2/\mu_1 = 0.5$)

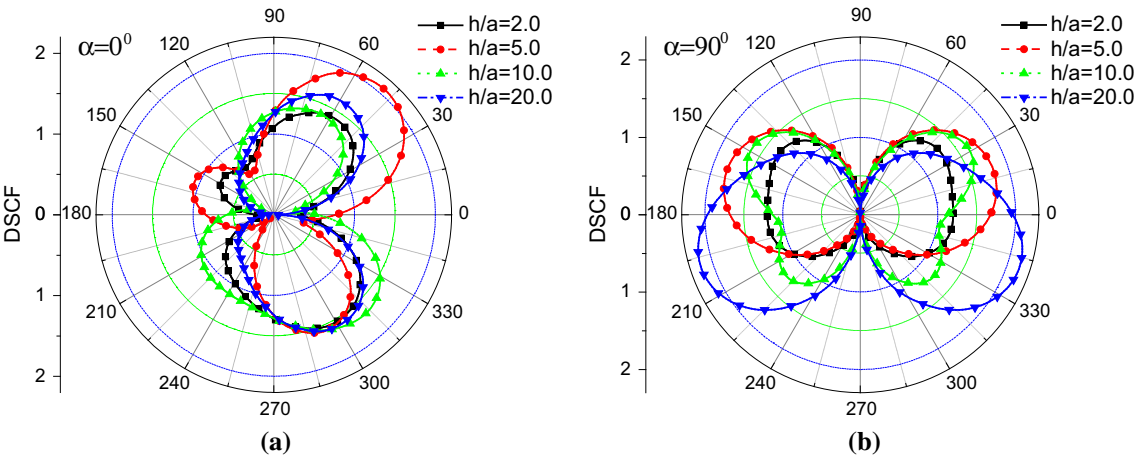

Fig. 8 Variation of DSCF with h/a ($a = 1.0$, $b = 0.8$, $h_1/a = 3.0$, $c = -1.0$, $2A = 2.0$, $\beta = 30°$, $k_2/k_1 = 0.5$, $\mu_2/\mu_1 = 0.5$)

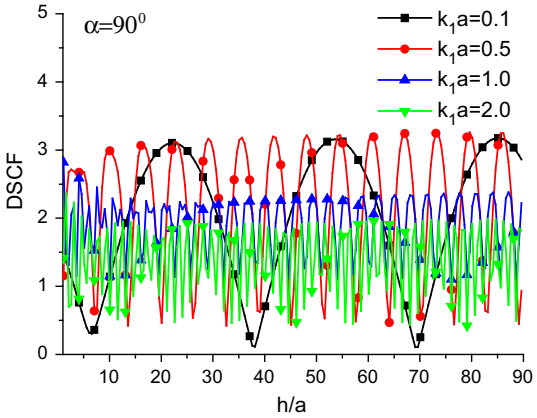

Fig. 9 Variation of DSCF at $\theta = 0°$ with $2A$ ($a = 1.0, b = 0.8, h_1/a = 3.0, c = -1.0, \beta = 30°, k_2/k_1 = 0.5, \mu_2/\mu_1 = 0.5$)

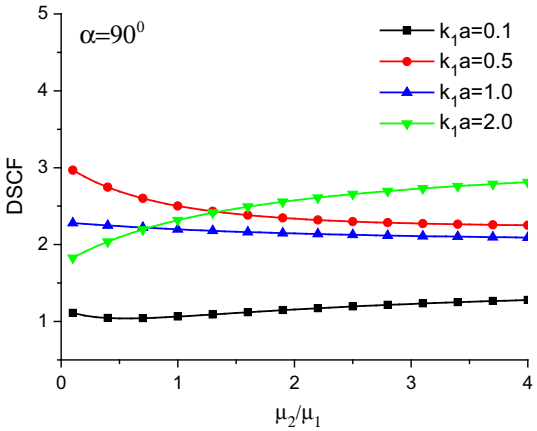

Fig. 10 Variation of DSCF at $\theta = 0°$ with $\mu_2/\mu_1 (a = 1.0, b = 0.8, h/a = 3.0, h_1/a = 3.0, c = -1.0, 2A = 2.0, \beta = 30°, k_2/k_1 = 0.5)$

The distribution curves of DSCF at $\theta = 0°$ of the elliptical cavity versus h/a and μ_2/μ_1 for the wave numbers of $k_1a = 0.1, 0.5, 1.0$ and 2.0 under vertically incident SH-waves are plotted in Figs. 9 and 10. Figure 9 reveals that $\tau^*_{\theta z}$ varies periodically with increasing h/a, and moreover, the larger the frequency of the incident wave (namely the wave number k_1a), the more intensely the variation of $\tau^*_{\theta z}$, but the lower its values. As illustrated in Fig. 10, the variation of μ_2/μ_1 impacts a little on the distribution of $\tau^*_{\theta z}$, and as μ_2/μ_1 increases, the value of $\tau^*_{\theta z}$ grows slowly for high frequency ($k_1a = 2.0$).

2. The variation law of DSIFs at the crack tip with different parameters under incident SH-waves with different angles is discussed in Figs. 11, 12, 13, 14 and 15.

Figure 11 gives the variation curves of k_3 with the frequency k_1a for the ratio of two shear modulus values of $\mu_2/\mu_1 = 0.1$, 1.0, 2.0 and 4.0. The variation curve of k_3 first has a sudden drop and then tends to be stable toward the higher frequency k_1a range. Comparing the results obtained in Fig. 11a, b shows that the values of k_3 decrease as k_1a increases for oblique incidence and has certain ion in other cases. Moreover, it can be also demonstrated from the data graph that μ_2/μ_1 impacts little on k_3.

From Fig. 12, as h/a gradually increases, the distribution curve of k_3 always drops suddenly and then tends toward periodic variation when SH-waves incident with different angles. Besides, the increase of the incident angle α leads to the decrease of k_3, and the maximum order is 4.75, 3.92 and 2.49 for $\mu_2/\mu_1 = 0.1$. The plots show that the dependence of the DSIF curve on the incident angle α is strongly impacted by the distance between the center of the cavity and the horizontal interface. It can be observed from Fig. 13 that the relative location of the crack leads to large variation in the values of k_3. With the increase of h_1/a, the value of k_3 sharply declines first and then diminishes with a smooth curve for $k_2/k_1 = 0.1$, while decays periodically for other cases, as demonstrated in Fig. 13.

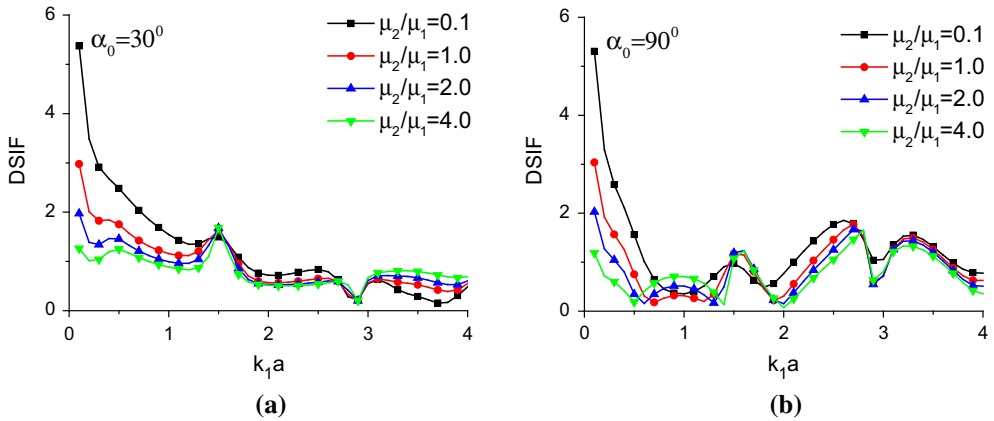

Fig. 11 Variation of DSIF with k_1a ($a = 1.0$, $b = 0.8$, $h/a = 3.0$, $h_1/a = 3.0$, $c = -1.0$, $2A = 2.0$, $\beta = 30°$, $k_2/k_1 = 0.5$)

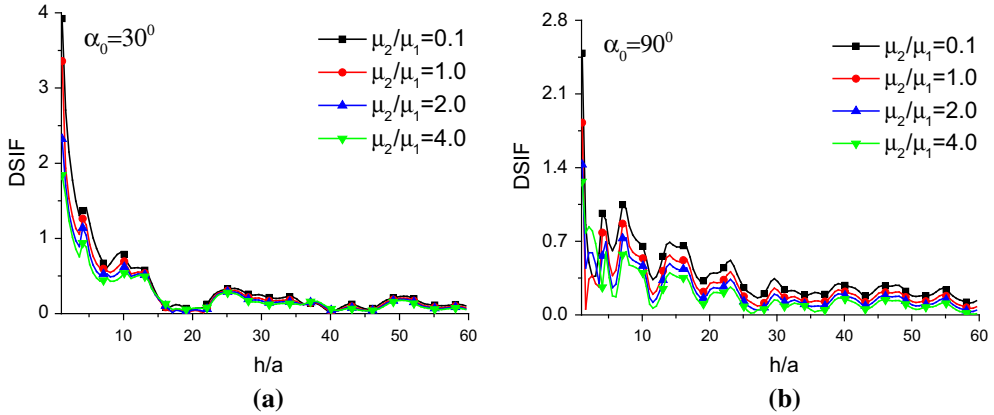

Fig. 12 Variation of DSIF with h/a ($a = 1.0$, $b = 0.8$, $h_1/a = 3.0$, $c = -1.0$, $2A = 2.0$, $\beta = 30°$, $k_1a = 1.0$, $k_2/k_1 = 0.5$)

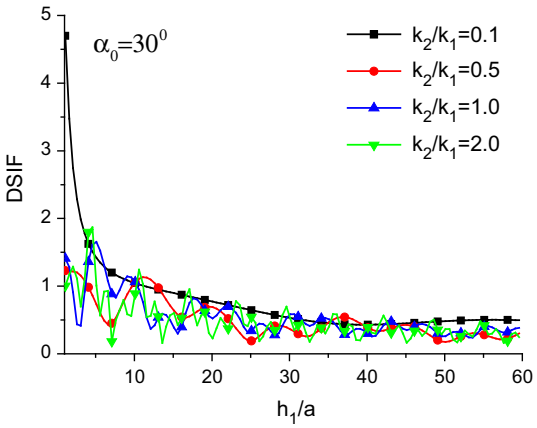

Fig. 13 Variation of DSIF with h_1/a ($a = 1.0$, $b = 0.8$, $h/a = 3.0$, $c = -1.0$, $2A = 2.0$, $\beta = 30°$, $k_1a = 1.0$, $\mu_2/\mu_1 = 0.5$)

Figure 14 investigates the influence of the ratio of two incident frequencies (namely the ratio of two wave numbers k_2/k_1) on the distribution of k_3. It can be pointed out that, as k_2/k_1 increases, the value of k_3 first declines and then tends to be a stable periodic variation. Moreover, the higher μ_2/μ_1 is, the large the value of k_3 becomes. When the incident angle α increases, the value of k_3 decreases.

A large influence of the vertical distance between the left-hand member of the crack and the center of the cavity c on k_3 is depicted in Fig. 15. By comparison of the three graphs, it can be concluded that the increase

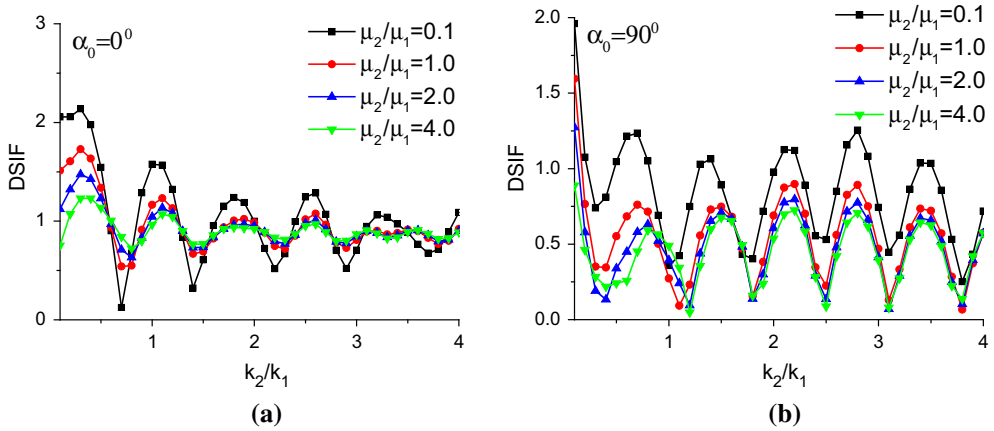

Fig. 14 Variation of DSIF with k_2/k_1 ($a = 1.0, b = 0.8, h/a = 3.0, h_1/a = 1.0, c = -1.0, 2A = 2.0, \beta = 30°, \mu_2 = 1.0, k_1 a = 1.0$)

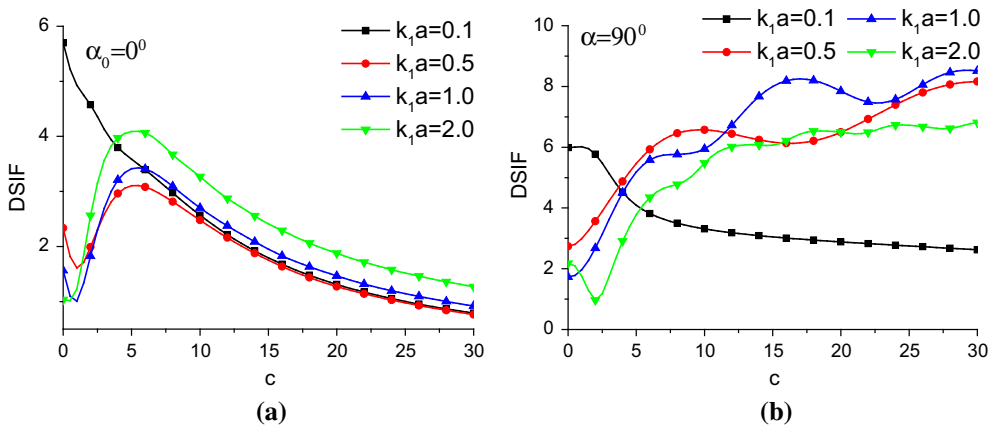

Fig. 15 Variation of DSIF with c ($a = 1.0, b = 0.8, h/a = 3.0, h_1/a = 2.0, 2A = 2.0, \beta = 0°, k_2/k_1 = 0.5, \mu_2/\mu_1 = 0.5$)

in the incident angle values leads to an amplification in the values of k_3 for $c \geq 6.0$ but a small change for $c \leq 6.0$. For $k_1 a = 0.1$, namely quasi-static, the value of k_3 is inversely but directly proportional to c in the cases of higher frequency while the SH-wave is incident vertically.

9 Conclusions

In the current paper, the methods of Green's function and complex variables were applied on the SH-waves scattering problem by an elliptical cavity and a crack, which are located in different media near bimaterials interface. Comprehensive numerical results were presented to discuss the influence of different parameters on the dynamic stress concentration factor (DSCF) around the elliptical and dynamic stress intensity factor (DSIF) at the crack tip, and some conclusions are summed up:

(i) In the numerical examples solved here, it can be revealed that the interface interaction effect is clearly manifested and different incident parameters such as $k_1 a$, α and h/a can lead to different distributions of $\tau^*_{\theta z}$ around the elliptical cavity. Compared with values obtained for $\alpha = 0°$, h/a yields a much more complicated variation of $\tau^*_{\theta z}$ when SH-waves incident obliquely or vertically. When $\alpha = 90°$, the values of $\tau^*_{\theta z}$ is are direct proportion to h/a.

(ii) The distribution of DSIF at the crack tip is impacted strongly by α, $k_1 a$, c, k_2/k_1, h/a and h_1/a. Specifically, the distance between the center of the cavity and the horizontal interface h/a strongly impacts on the dependence of the DSIF with incident angles α. Additionally, the increase in the incident angle values leads to amplification in the values of k_3 for $c \geq 6.0$ but small change for $c \leq 6.0$.

(iii) The model of irregularly shaped cavities and cracks near bimaterials interface is common in practical engineering, such as oil exploration, underground tunnel engineering, mineral resources exploration, QNDE, radar, sonar and explosion. Thus, the mechanics law (influence of different parameters on dynamics response of complex defects near bimaterials interface) revealed by the obtained exact solution in this paper will be a useful reference for engineering practice and the study on material properties.

(iv) The methods presented in this paper can be developed for further study on the dynamic response problem of more complicated irregularly shaped cavity and crack near bimaterials interface but not be applied to the model of a cavity with a through crack. The key is to use the technique of "conformal mapping" in complex variables to map the complicated irregular boundary of the cavity to the unit circle boundary under satisfying the accuracy of the zero-stress condition at the cavity boundary.

(v) Based on this report, the study of the SH-waves scattering problem by multiple elliptical cavities and multiple cracks near bimaterials interface can be extended for future study.

Acknowledgments This project was supported by Earthquake Industry Special Science Research Foundation Project (No. 20150 8026-02), the Natural Science Foundation of Heilongjiang Province of China (No. A201310), the Scientific Research Starting Foundation for Post Doctorate of Heilongjiang Province (No. LBHQ13040), and the Scientific Starting Research Foundation for Doctor, Longyan University (No. LB2014012).

References

1. Pao, Y.H., Mow, C.C.: Diffraction of elastic waves and dynamic stress concentrations. pp. 114–304. Crane and Russak, New York (1973)
2. Liu, D.K., Gai, B.Z., Tao, G.Y.: Applications of the method of complex variables to dynamic stress concentrations. Wave Motion **4**, 293–304 (1982)
3. Chen, T.Y., Wang, H.: Dynamic analysis of upright incident of SH-waves at semi-cylindrical interface with a circular lining structure. J. Tianjin Univ. **39**, 1305–1309 (2006)
4. Wang, G.Q., Liu, D.K.: Scattering of SH-wave by multiple circular cavities in half space. Earthq. Eng. Eng. Vib. **1**, 36–44 (2002)
5. Xu, P., Tie, Y., Xia, T.D.: Scattering of plane SH Waves by two separated circular tunnel linings. Northwest. Seismol. J. **30**, 145–149 (2008)
6. Liu, D.K., Lin, H.: Scattering of SH-waves by circular cavities near biomaterial interface. Acta Mech. Solida Sin. **24**, 197–204 (2003)
7. Liu, D.K., Lin, H.: Scattering of SH-waves by an interface linear crack and a circular cavity near bimaterial interface. Acta Mech. Sin. **20**, 317–326 (2004)
8. Yang, Z.L., Chen, Z.G., Liu, D.K.: Scattering of SH-wave by an interacting mode III crack and a circular cavity in half space. Key Eng. Mater. **348**–**349**, 861-864 (2007)
9. Yang, Z.L., Yan, P.L., Liu, D.K.: Scattering of SH-waves and ground motion by an elastic cylindrical inclusion and a crack in half space. Chin J. Theor. Appl. Mech. **41**, 229–235 (2009)
10. Lu, J.F., Wang, Y.S., Cai, L.: Scattering of SH wave by a crack terminating at the interface of bi-material. Chin J. Theor. Appl. Mech. **35**, 432–436 (2003)
11. Rodriguez-Castellanos, A., Luzon, F., Sanchez-Sesma, F.J.: Diffraction of seismic waves in an elastic cracked half plane using boundary integral formulation. Soil Dyn. Earthq. Eng. **25**, 827–837 (2005)
12. Tsaur, D.H., Chang, K.H.: Multiple scattering of SH waves by an embedded truncated circular cavity. J. Mar. Sci. Technol. **20**, 73–81 (2012)
13. Wang, Y.S., Qiu, Z.Y., Yu, G.L.: Scattering of SH waves from a partially debonded rigid elliptic cylinder. Soil. Dyn. Earthq. Eng. **21**, 139–149 (2001)
14. Coussy, O.: Scattering of elastic waves by an inclusion with an interface crack. Wave Motion **6**, 223–236 (1984)
15. Bair, V.B., David, B.B.: Wave scattering by surface-breaking cracks and cavities. Wave Motion **40**, 163–172 (2004)
16. Tanimura, S.: Stress wave propagation in elastic/viscoplastic cylindrical bodies containing a spherical cavity. Acta Mech. **51**, 1–13 (1984)
17. Yu, C.W., Dravinski, M.: Scattering of plane harmonic P, SV and Rayleigh waves by a completely embedded corrugated elastic inclusion. Wave Motion **47**, 156–167 (2010)
18. Dravinski, M., Sheikhhassani, R.: Scattering of a plane harmonic SH wave by a rough multilayered inclusion of arbitrary shape. Wave Motion **50**, 836–851 (2013)
19. Parvanova, S., Dineva, P., Manolis, G.D.: Elastic wave fields in a half-plane with free-surface relief, tunnels and multiple buried inclusions. Acta Mech. **225**, 1843–1865 (2014)